

# Interference phenomena in the $J^P = 1/2^-$ -wave in $\eta$ photoproduction

A.V. Anisovich<sup>1,2</sup>, E. Klempt<sup>1</sup>, B. Krusche<sup>3</sup>, V.A. Nikonov<sup>1,2</sup>, A.V. Sarantsev<sup>1,2</sup>, U. Thoma<sup>1</sup>, D. Werthmüller<sup>3</sup> <sup>a</sup>

<sup>1</sup> Helmholtz-Institut für Strahlen- und Kernphysik, Universität Bonn, Germany

<sup>2</sup> Petersburg Nuclear Physics Institute, Gatchina, Russia

<sup>3</sup> Departement für Physik, Universität Basel, Switzerland

Received: July 26, 2021/ Revised version:

**Abstract.** The recent precise experimental results for the photoproduction of  $\eta$ -mesons off the neutron measured with the Crystal Ball/TAPS calorimeter at the MAMI accelerator have been investigated in detail in the framework of the Bonn-Gatchina coupled channel model. The main result is that the narrow structure observed in the excitation function of  $\gamma n \rightarrow n\eta$  can be reproduced fully with a particular interference pattern in the  $J^P = 1/2^-$  partial wave. Introduction of the narrow resonance  $N(1685)$  with the properties reported in earlier publications deteriorates the quality of the fit.

## 1 Introduction

So far photoproduction of mesons off the neutron has been much less investigated than the corresponding reactions off the free proton. The reasons are the obvious difficulties related to measurements using nucleons bound in nuclei (in most cases neutrons bound in the deuteron) as targets. There are not only the technical complications arising from the necessity to detect the recoil neutrons but also the difficulties in the interpretation of the results which are effected by nuclear Fermi motion and Final State Interaction (FSI) effects. Nevertheless, such reactions are important because they reveal the isospin structure of the electromagnetic excitation currents. The coupling of isospin  $I = 3/2$   $\Delta$  resonances to  $\gamma N$  is identical for protons and neutrons, but the  $\gamma N \rightarrow N^*$  couplings are isospin dependent. During the last few years quite some progress has been made for this branch of the photonuclear experimental program [1] and first results have been reported for several reaction channels. The measurements of  $\eta$  photoproduction off the neutron have attracted particular interest, because around 1 GeV of incident photon energy ( $W \approx 1680$  MeV) a narrow structure was observed in the excitation function [2,3,4]. These observations are listed by the Particle Data Group [5] as one-star nucleon resonance  $N(1685)$ . Remarkably, such a structure had been predicted by soliton models in the context of the conjectured baryon antidecuplet of pentaquarks. The nonstrange member of the multiplet with spin-parity  $J^P = 1/2^+$  [6] should be electromagnetically excited more strongly on the neutron, should have a large decay branching ratio to

$N\eta$ , an invariant mass around 1.7 GeV, and a width of a few tens of MeV [6,7,8,9]; all properties that are phenomenologically exhibited by the observed structure. If one treats this structure as a single isolated resonance, a mass of  $1670 \pm 5$  MeV and a width of  $\Gamma \approx 30$  MeV are determined. Assuming a constant angular distribution ( $J^P = 1/2^+$  or  $1/2^-$ ) and ignoring possible interference effects, the electromagnetic coupling strength is determined to  $A_{1/2} \cdot \sqrt{b_\eta} \approx 12 \times 10^{-3}$  GeV<sup>-1/2</sup> [4] or, respectively, to  $(12.3 \pm 0.8) \times 10^{-3}$  GeV<sup>-1/2</sup> [10]. The radiative width derived by Azimov *et al.* [11] using the GRAAL data [2] corresponds to  $A_{1/2} \cdot \sqrt{b_\eta} = 15 \times 10^{-3}$  GeV<sup>-1/2</sup>. The experimental values for the properties of  $N(1685)$  are all in the predicted range for the nonstrange partner of the  $\Theta^+$ , an exotic baryon which was “discovered” in 2003. Shortly after, the evidence for its existence faded away in a number of precision experiments [12,13,14] but evidence is reported in several more recent experiments [15], [16] (see, however, [17]), and [18].

In contrast to the history of the exotic  $\Theta^+$  pentaquark, the statistical significance of the structure observed in  $\gamma n \rightarrow n\eta$  is undisputable. All experiments that searched for this structure came out with positive results, and the most recent measurements at the MAMI accelerator with deuterium [10,19] and also <sup>3</sup>He targets [19,20] established it beyond any doubts. Due to the full kinematic reconstruction of the  $\eta$  - neutron final state, effects from nuclear Fermi motion - smearing out narrow structures - were removed so that a better estimate of the width of the structure became possible [10,19]. Monte Carlo simulations showed that the observed width of  $50 \pm 10$  MeV (the natural width folded with the experimental resolution) corresponds to a natural width of only  $\approx 30$  MeV. Such

<sup>a</sup> Present address: School of Physics and Astronomy, University of Glasgow, Glasgow G12 8QQ, United Kingdom

a narrow width would be very unusual for a normal three-quark nucleon resonance with a mass of  $W \approx 1680$  MeV. There is a possibly correlated, although very weak effect, in  $\gamma p \rightarrow \eta p$  [21] where a narrow dip is observed at the same incident photon energy. An observation has also been reported for Compton scattering  $\gamma n \rightarrow \gamma n$  [22]. A measurement of the beam asymmetry  $\Sigma$  for Compton scattering off protons suggested even two narrow structures with masses near 1680 and 1.720 MeV [23].

We have thus the awkward situation that a resonance was predicted at about 1680 MeV in the soliton model, and a bump-like structure with exactly the right properties was found in experiments. However, there are serious doubts that this bump is related to the predicted pentaquark state. Here, one should not forget that not each bump observed in some excitation function is evidence for a resonance. There can be other effects, for example threshold cusps. In fact, it has already been tried to model this bump with various approaches. Apart from intrinsically narrow states [9,24,25,26,27], different coupled-channel and interference effects of known nucleon resonances have been discussed in the literature. The Gießen group claimed that the narrow peak in the  $\eta$  photoproduction on the neutron can be explained as  $N(1650)1/2^-$  and  $N(1710)1/2^+$  coupled-channel effect [28]; Shyam and Scholten use interference effects between the  $N(1650)1/2^-$ ,  $N(1710)1/2^+$ , and  $N(1720)3/2^+$  resonances to describe the peak [29], Döring and Nakayama ascribe the peak to effects from strangeness threshold openings [30]. The Bonn-Gatchina group demonstrated that the narrow peak can be explained naturally by interference effects in the  $J^P = 1/2^-$  wave [27], a conclusion which was confirmed independently - even though three years later - by Zhong and Zhao [31].

Here, we come back to the idea first put forward in [27] where two different scenarios for the bump structure in the CBELSA  $\gamma n \rightarrow n\eta$  data [3] were discussed. In the first scenario, the two resonances with spin-parity  $J^P = 1/2^-$  -  $N(1535)1/2^-$  and  $N(1650)1/2^-$  - and the interference between them was studied; this ansatz gave a good fit to the data. In the second scenario, a narrow resonance at 1685 MeV and with photo-coupling and  $N\eta$  decay branching ratio as predicted in [6,7,8,11] was introduced; this model gave a fit of equivalent quality. Thus the existence of  $N(1685)$  was not supported but could not be ruled out. This situation has now completely changed with the new, very precise data measured by the Crystal Ball/TAPS experiment at MAMI [10,19]. In this paper we compare fits to the new data with the two scenarios discussed above and find a much better description without introduction of the  $N(1685)$  resonance, which makes the interpretation of the bump-like structure as resonance improbable.

In the experimental publications describing the new data [10,19], the same strongly simplified model as in [3,4] was used. The model consists of a superposition of three Breit-Wigner functions without interference terms. The Breit-Wigner functions represent i) the narrow structure, ii) the  $N(1535)1/2^-$  standing for the full  $J^P = 1/2^-$  partial wave, and iii) the background contributions. The

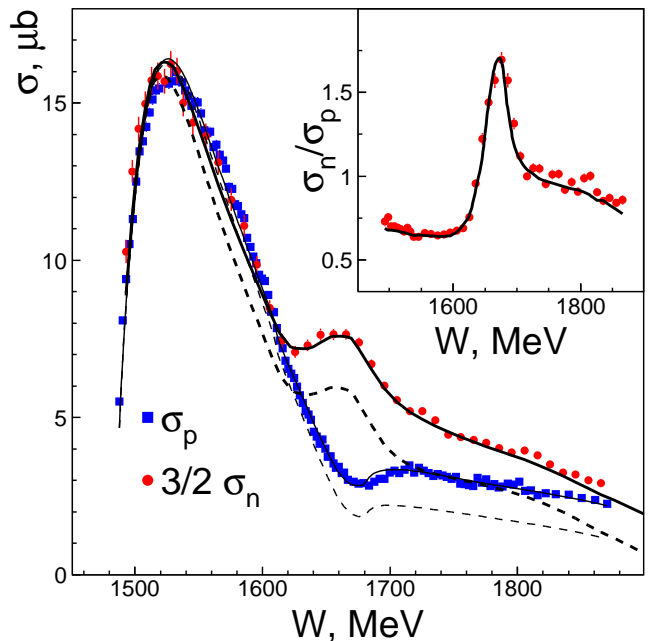


**Fig. 1.** (color online) The total cross section for  $\gamma n \rightarrow \eta n$ ,  $\gamma p \rightarrow \eta p$ , and their ratio as functions of the  $\eta N$  invariant mass. The solid curves represent our final fits, dashed curves the  $J^P = 1/2^-$  contributions.

model served to extract phenomenological estimates for position and width of the observed bump.

It is obvious that a much refined analysis of the data is necessary and this is possible within the Bonn-Gatchina coupled channel approach, which was recently updated for reactions off neutrons [32]. This paper discusses in detail new fits to the data within different scenarios and their implication to the nature of the observed structure. A comment-like short version of part of this analysis is already available on the arXiv [33].

The paper is organized as follows. In section 2 we summarize the experimental data used in this paper. Subsequently (section 3), we present some simulations; the aim is to introduce to the reader the patterns which may emerge from known input into a partial wave analysis. In section 4 we present our fits to the data imposing or not imposing the presence of a narrow resonance in the  $J^P = 1/2^+$  wave. A short summary is given at the end.

## 2 Data used in this analysis

The main new data used in this paper are the  $\gamma n \rightarrow \eta n$  differential cross section from MAMI [10,19]. The data – shown in Fig. 1 – were taken with a deuteron target but with full event reconstruction. Therefore these data do not suffer from the Fermi motion which usually smears out narrow structures in the cross section. The new  $\gamma n \rightarrow n\eta$  data obtained also at MAMI with a  $^3\text{He}$  target [19,20] are consistent with the deuteron data apart from the absolute scale which is influenced by FSI. They were therefore not

included into the fits. In addition to these data we use GRAAL data on the beam asymmetry  $\Sigma$  for  $\gamma n \rightarrow \eta n$  [41]. The precision data from MAMI on  $\gamma p \rightarrow \eta p$  [21] are discussed to clarify the underlying physical processes. The shallow dip at 1680 MeV in the  $\gamma p \rightarrow p\eta$  cross section reported in [21] was described by introducing  $N(1685)$  or by assuming that there is a large  $\omega$  coupling to the  $J^P = 1/2^-$  wave [37]. For pion production, the data on  $\gamma d \rightarrow \pi^0 n p_{\text{spectator}}$  and on  $\pi^- p \rightarrow \gamma n$  listed in Table 1 of [32] and the recent data from MAMI [34] on  $\gamma d \rightarrow \pi^0 n p_{\text{spectator}}$  were used.

In all fits presented here, masses, widths and coupling constants for the decay of nucleon resonances are fixed except those for helicity amplitudes of resonances and those for  $t$  and  $u$ -channel exchange amplitudes. The fixed values are taken from our fits to a large body of  $\pi N$  elastic scattering and pion and photo-induced inelastic reactions (see [35,36] for references to the data included).

### 3 Simulations

Before we present the results of the partial wave analysis, we present some simulations which demonstrate what to expect given a particular hypothesis. The simulations are close to the experimental observations but the underlying model is simpler and focuses on specific aspects of the reaction.

#### 3.1 Simulation of the narrow structure with $J^P = 1/2^-$ and $J^P = 1/2^+$ states

First we study the interference between a dominant  $J^P = 1/2^-$  wave and a narrow resonance in the  $J^P = 1/2^+$  wave. A typical example is shown in Fig. 2. Two contributions are present:  $N(1535)$  provides a strong  $J^P = 1/2^-$  wave at low energies, a narrow  $J^P = 1/2^+$  resonance with a mass of 1680 MeV forms the second peak in the total cross section.

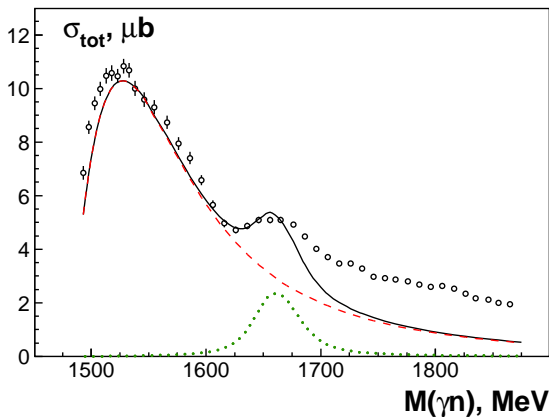


**Fig. 2.** (color online) Simulation of the total cross section (solid line) with contributions from  $J^P = 1/2^-$  (dashed curve, red) and  $J^P = 1/2^+$  (dotted curve, green).

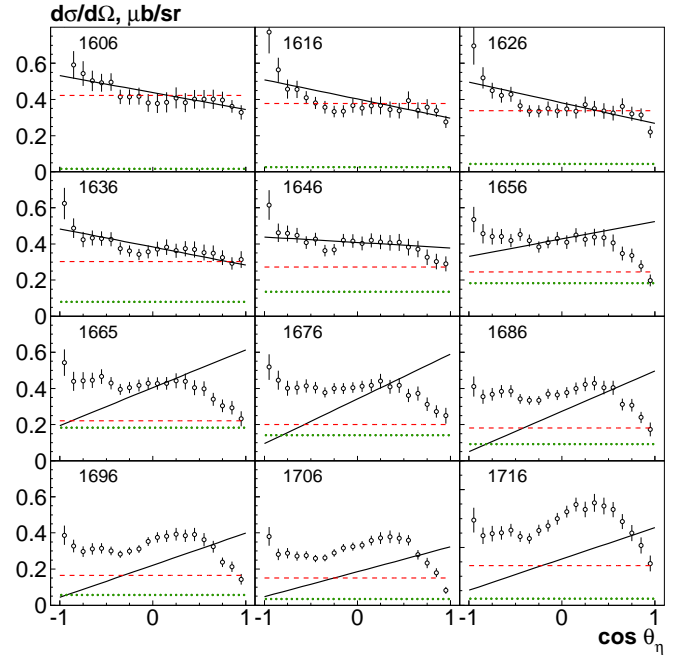


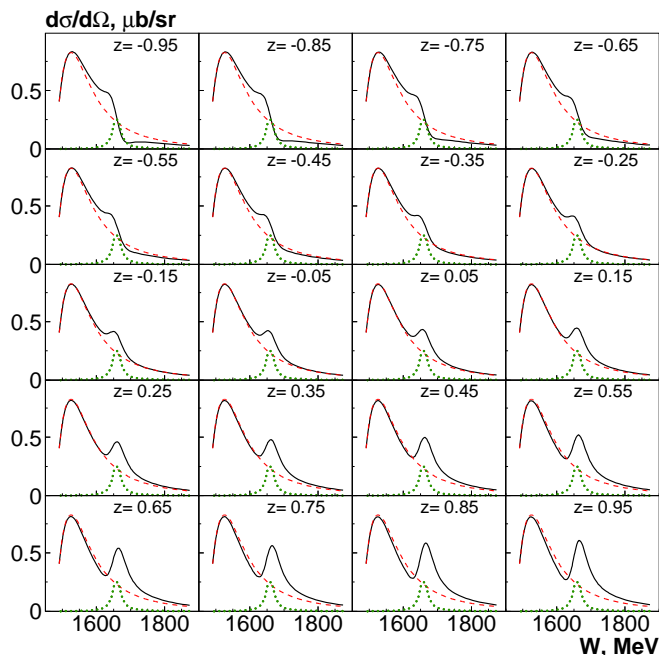
**Fig. 3.** (color online) Differential cross section for the eta photoproduction with (solid curve) and without interference between  $J^P = 1/2^-$  (dashed curve, red) and  $J^P = 1/2^+$  (dotted curve, green) waves. The numbers correspond to the central mass of a bin (in MeV).

Without interference, both partial waves produce uniform angular distributions, see the dashed (red) and dotted (green) curves in Fig. 3. The interference between the two waves generates a linear angular distribution; its slope depends on the phase between the  $J^P = 1/2^-$  and  $J^P = 1/2^+$  waves. Overall, the area below the solid line is larger than the area below the dashed line: the narrow  $J^P = 1/2^+$  resonance brings in additional intensity. However, in most energy bins there are angular regions where the solid line is below the dashed one. These are regions of strong destructive interference.

The excitation functions at fixed angles are shown in Fig 4. The distributions show either a peak at the mass of the  $J^P = 1/2^+$  resonance or a diffractive pattern. We will see that the data are inconsistent with these assumptions. Note that the total cross section can be calculated from the differential cross section and from the excitation function by calculating the mean of all  $\cos \theta$  bins and multiplying with  $4\pi$ .

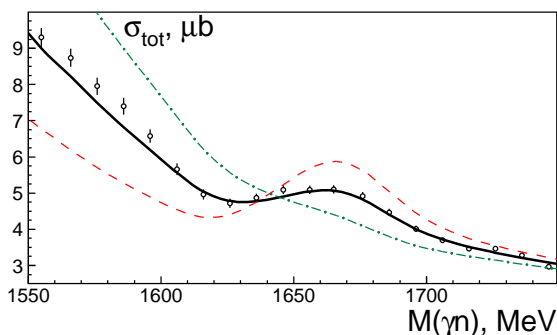
#### 3.2 Simulation of the interference pattern

Figure 5 shows a simulation of the effect of the interference between the two  $J^P = 1/2^-$  resonances. The solid curve represents our best fit (as discussed below). The  $J^P = 1/2^-$  wave is represented by a K-matrix with three poles and smooth background [27] (which contributes less than 10% to the cross section). Then we have multiplied the  $A_{1/2}^n$  helicity amplitude of  $N(1650)1/2^-$  with a factor 2 or (-1). This has a very significant impact on the pre-



**Fig. 4.** (color online) Energy distributions at fixed angles (in bins of  $z = \cos \Theta_\eta$ ) in the case of the interference between  $J^P = 1/2^-$  and  $J^P = 1/2^+$  states. The contributions of the  $J^P = 1/2^-$  partial wave are shown with dashed (red) curves and  $J^P = 1/2^+$  with dotted (green) curves.

dicted cross section. When the  $N(1650)1/2^-$  helicity amplitude is increased (from  $0.019$  to  $0.038 \cdot 10^{-3} \text{ GeV}^{-1/2}$ ), the peak structure grows significantly while only a small effect remains visible when the sign of the helicity amplitude is changed.



**Fig. 5.** (color online) The total cross section for  $\gamma n \rightarrow \eta n$  [19] with our best fit (solid curve) and with predictions in which the helicity amplitude  $A_{1/2}^n$  of  $N(1650)1/2^-$  is multiplied by a factor 2 (dashed, red) or -1 (dashed-dotted, green), respectively.

### 3.3 Simulation of a cusp

We show the effect of the opening of a new channel using data on  $\gamma p \rightarrow \eta p$ . For this reaction a small dip in the total cross section at about  $1.68 \text{ GeV}$  was reported [21].

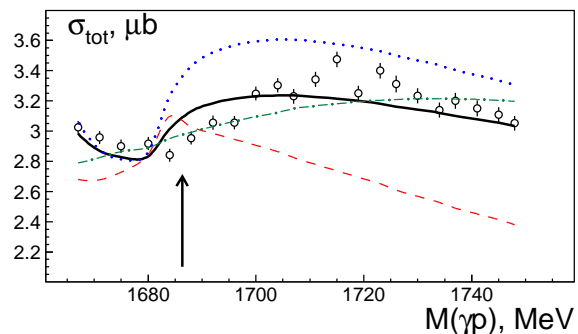


**Fig. 6.** (Color online) Total cross section for  $\gamma p \rightarrow \eta p$ . Solid (black) curve: best fit; dashed-dotted (green) curve: fit with zero coupling to the  $K\Sigma$  final state; dotted (blue) curve: coupling of  $N(1650)1/2^- \rightarrow K\Sigma$  doubled; dashed (red) curve: coupling of  $N(1650)1/2^- \rightarrow K\Sigma$  with negative sign. The arrow indicates the position of the  $K\Sigma$  threshold.

The structure was soon assigned to the narrow nucleon resonance  $N(1685)$  [38]. A detailed study showed that the structure can be described well when the  $N(1685)$  nucleon resonance with spin-parity  $J^P = 1/2^+$  is added to the list of resonances used in the BnGa partial wave analysis [37]. However, an equally good fit was obtained when taking into account the opening of the reaction  $\gamma p \rightarrow p\omega$  at  $1720 \text{ MeV}$ .

At the time when the study [37] was made, data on photoproduction of  $\omega$  mesons were not yet included in the BnGa analysis. With such data included, it turned out that the  $p\omega$  coupling of the  $J^P = 1/2^-$  partial wave would need to be considerably larger than the data on  $\gamma p \rightarrow p\omega$  suggest. Hence we decided to study the effect of the opening of the reaction  $\gamma p \rightarrow K\Sigma$ . In a recent analysis, we reported an ambiguity in the signs of  $N \rightarrow K\Sigma$  coupling constants [36]. The new solution (BnGa2013-02) had a much more significant  $J^P = 1/2^-$  contribution than the solution (BnGa2011-02M), see Fig. 12 of [36] and is in an excellent agreement with the solution found by Rönchen *et al.* [39]. Based on the new solution, the total cross section for  $\gamma p \rightarrow \eta p$  should exhibit a clear structure at the  $K\Sigma$  threshold which is shown in Fig. 6. This is the case, indeed. The figure shows the expected distribution (solid curve) and curves which are predicted for the case of vanishing  $K\Sigma$  coupling, for a coupling multiplied by a factor 2, and for a factor (-1). The solid line does not match the data points exactly but the effect of the  $K\Sigma$  threshold is clearly seen. Note that the errors correspond to statistical errors only. The importance of the  $K\Sigma$  coupling for the description of  $J^P = 1/2^-$  structure around  $1700 \text{ MeV}$  wave was stressed by M. Döring (see [40] and references therein).

## 4 Partial wave analysis of the data

We start our analysis from the solutions reported in [32]. These solutions were obtained by fitting almost the full data base on  $\gamma n \rightarrow \pi N$ ,  $\pi^- p \rightarrow \gamma n$ , and on  $\gamma n \rightarrow \eta n$ .

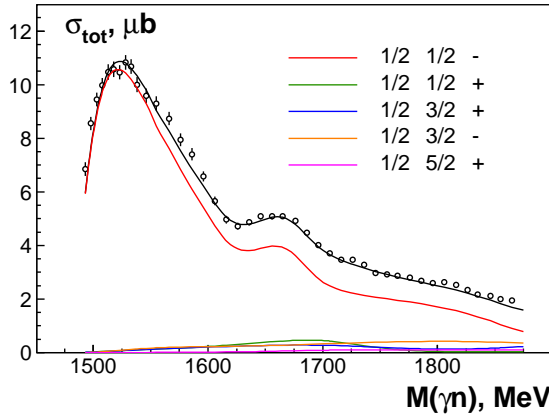


**Fig. 7.** (color online) The total cross section for  $\gamma n \rightarrow \eta n$  and the contributions from partial wave with isospin 1/2 and different spin-parities. There is no narrow  $N(1685)$  admitted in the fit. The structure at this mass is described by interference within the  $J^P = 1/2^-$  wave.

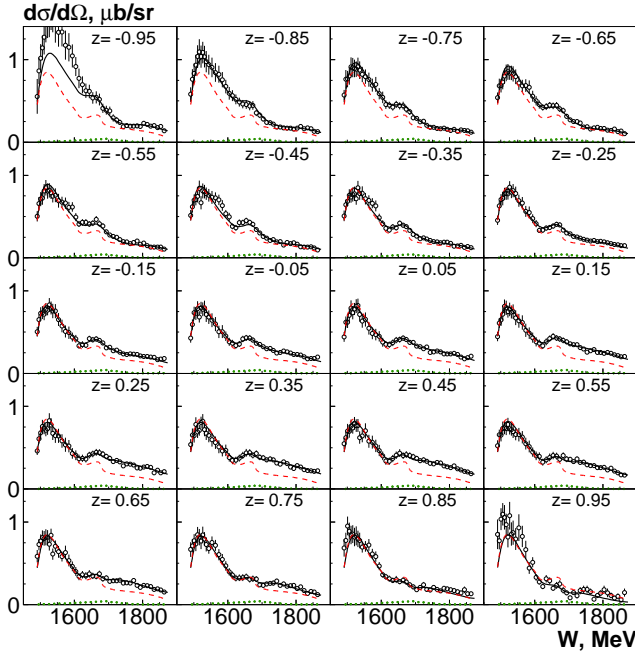


**Fig. 8.** (color online) Excitation function for  $\gamma n \rightarrow \eta n$  at fixed angles (in bins of  $z = \cos \Theta_\eta$ ). Only statistic errors are shown. There is no narrow  $N(1685)$  admitted in the fit. The fit is represented by the full (black) curve; the  $J^P = 1/2^-$  wave by the dashed (red) curve. The contributions from partial wave with isospin 1/2 and different spin-parities are shown by colored curves.

#### 4.1 Fits with no narrow nucleon resonance

First, we fitted the data with conventional nucleon resonances only. Figure 7 shows the total cross section with the fit and the most significant partial wave contributions. Clearly, the  $J^P = 1/2^-$  wave is dominant; the fit finds small contributions from the  $J^P = 1/2^+$ ,  $3/2^-$ ,  $3/2^+$ , and  $5/2^-$  waves. In the fit, we use statistical and systematic errors added quadratically. The fit returns  $\chi^2$  values per

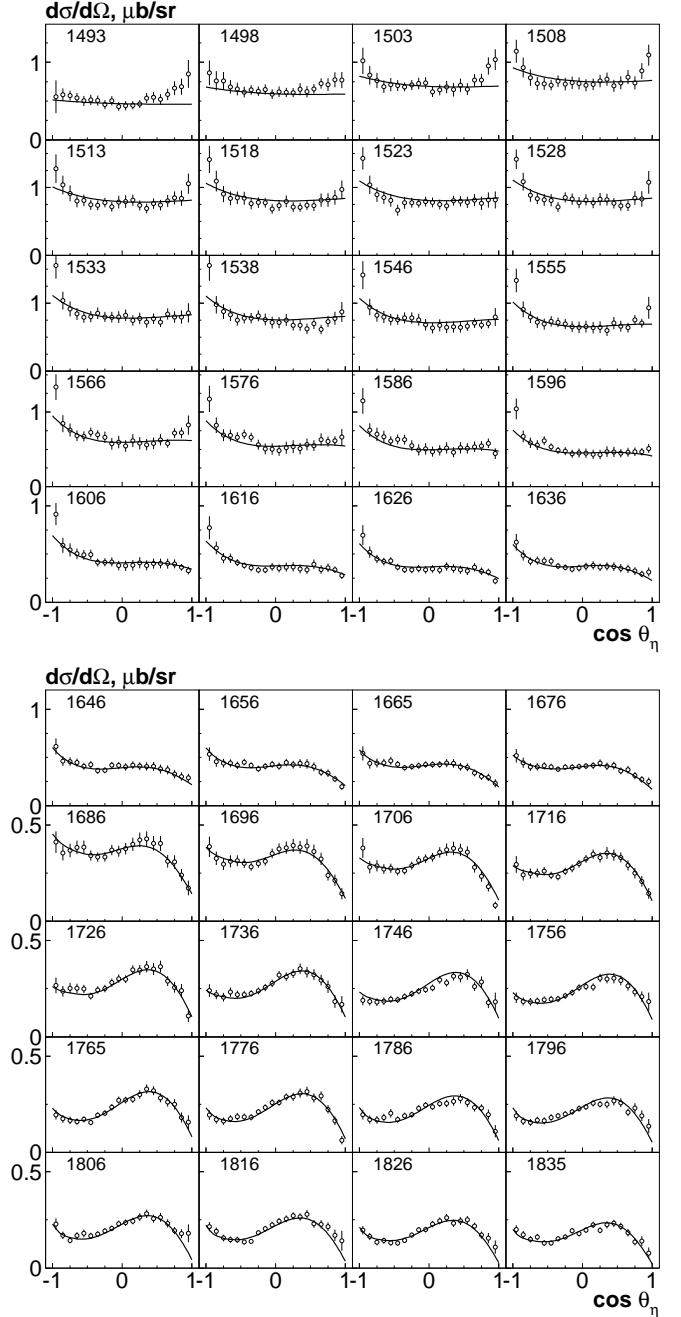


**Fig. 9.** (color online) Differential cross sections for  $\gamma n \rightarrow \eta n$ . Only statistic errors are shown. There is no narrow  $N(1685)$  admitted in the fit.

data point which are often smaller than 1. This is not surprising since several sources of systematic uncertainty vary slowly with energy or are constant. Using the statistical errors only, typical  $\chi^2$  values per data point are slightly above 3, indicating the need for error contributions beyond the statistical errors. The conclusions of the paper are not affected when the systematic errors are included or neglected.

The quality of the fit can be judged by inspecting Figs. 8 and 9. A  $\chi^2$  of 0.91 per data point was achieved.

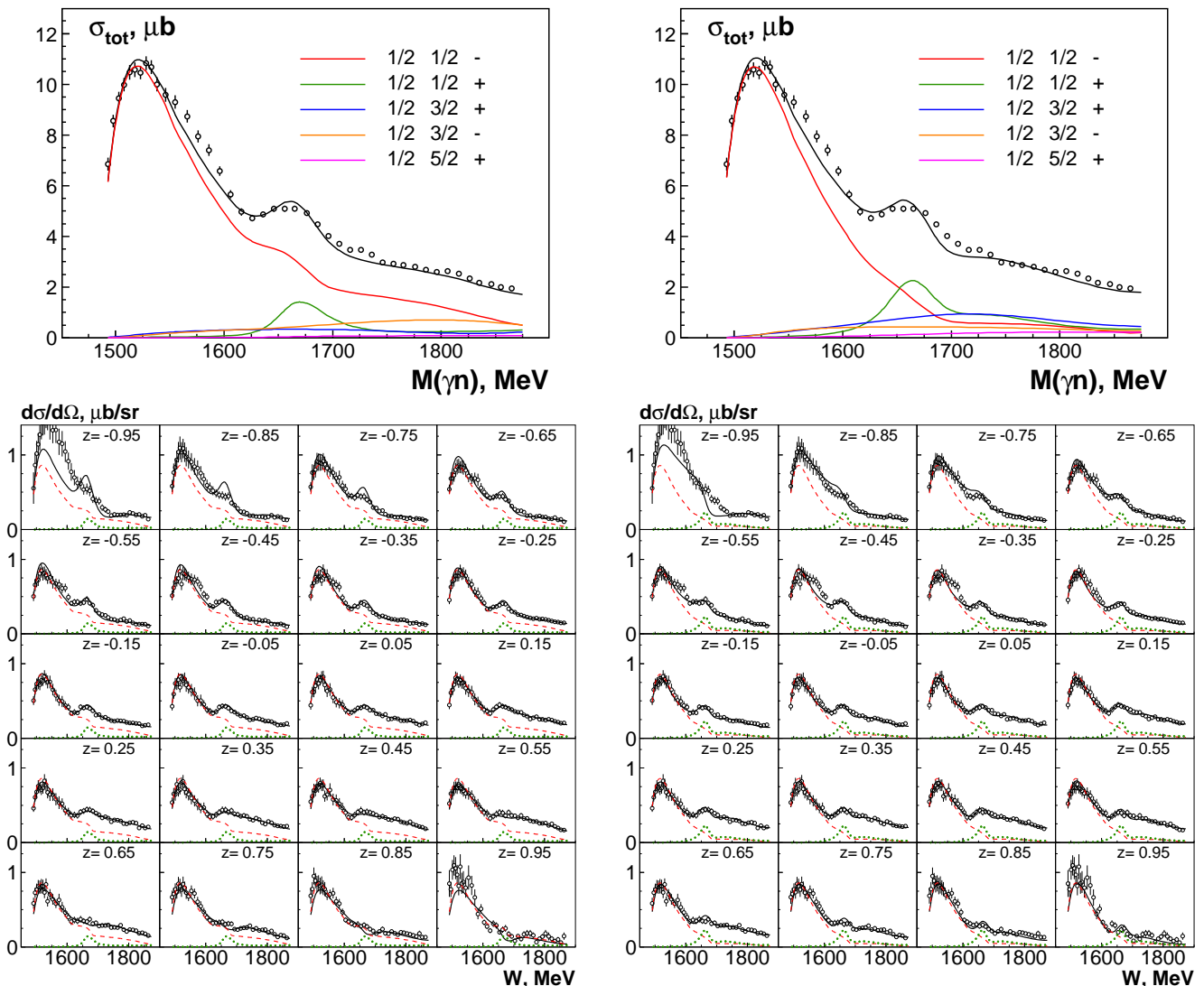


**Fig. 10.** (color online) Total cross section (top) and excitation functions at fixed angles (bottom). Only statistical errors are shown. In the fit a narrow  $J^P = 1/2^+$  resonance at 1685 MeV is imposed. Left:  $\tilde{a} > 0$ ; right:  $\tilde{a} < 0$  (see text).

A large fraction of the  $\chi^2$  stems from the most backward  $\eta$  production angle ( $z = \cos\theta = -0.95$ ). In Fig. 8, a significant excess of data compared to the fit is seen in this angular range at low energies ( $1520 < W < 1620$  MeV).

The angular distributions (Fig. 9) suggest that this excess might be artificial. In this mass range, most backward data points seem anomalously high. The detection efficiency for these points (see Fig. 13 in [10]) is much lower than for the second point in the angular distributions and the systematic uncertainty is larger. This small excess also explains the small discrepancy between data and fit in the total cross section around 1580 MeV (Figs. 1, 5, and 7). We conclude that an excellent fit to the data [10,19] can be achieved without introducing a narrow resonance  $N(1685)$ . In the 1610 - 1710 MeV mass region, the  $\chi^2$  per data point is 0.48.

#### 4.2 Fits imposing a narrow nucleon resonance $N(1685)$

In the next step we investigated the scenario with a narrow  $J^P = 1/2^+$  resonance interfering with the  $J^P = 1/2^-$  partial wave. We added a  $J^P = 1/2^+$  resonance in the 1680 MeV mass region. A fit with free width and real  $\eta n$  coupling converged to a solution with a very broad resonance (more than 200 MeV) and a very weak coupling. The improvement in  $\chi^2$  was negligible.

We then imposed contributions from a  $N(1685)$  resonance with properties corresponding to the phenomenologic fits in [19]: mass  $M = 1670 \pm 5$  MeV, width  $\Gamma = 30 \pm 15$  MeV, and  $\sqrt{Br(\eta n)} A_n^{1/2} = \tilde{a}$  [ $\text{GeV}^{-\frac{1}{2}} 10^{-3}$ ] =  $(12.3 \pm 0.8)$  [ $\text{GeV}^{-\frac{1}{2}} 10^{-3}$ ]. For  $\tilde{a}$  we assumed, alternatively, to have a positive or a negative sign. (When complex values were admitted, the overall  $\chi^2$  improved slightly

**Table 1.** (color online) Solutions with and without a contribution from a narrow resonance in the  $J^P = 1/2^+$  wave. The product of helicity coupling and  $\eta n$  branching ratio is given in units of  $\text{GeV}^{-\frac{1}{2}} 10^{-3}$ . The  $\chi_{dcs}^2$  for the differential cross section is calculated in the region 1.610 – 1710 MeV. The  $\chi_{\Sigma}^2$  for the beam asymmetry  $\Sigma$  is given separately. Results are given for two fits using only the statistical errors or the total errors.

Fit	Mass	Width	$\sqrt{Br(\eta n)} A_n^{1/2} $	Phase	$\chi_{dcs}^2/200$	$\chi_{\Sigma}^2/80$	$\chi_{dcs}^2/200$	$\chi_{\Sigma}^2/80$
					stat. + syst. errors	stat. errors only	stat. errors only	stat. errors only
$J^P = 1/2^-$	-	-	-	-	0.48	1.81	3.10	2.10
$J^P = 1/2^+$	1671	35	-12	$0^\circ$	1.34	2.80	9.35	2.92
$J^P = 1/2^+$	1669	35	+12	$0^\circ$	1.47	2.71	7.66	3.02
$J^P = 1/2^+$	1671	35	-12	$20^\circ$	1.50	2.50	9.33	2.90
$J^P = 1/2^+$	1674	35	5	$0^\circ$	0.55	1.98	3.40	2.50
$J^P = 1/2^+$	1671	35	-3	$0^\circ$	0.54	1.95	3.30	2.55

but the  $\chi^2$  restricted to the 1620 - 1720 MeV region was worse.)

The total cross sections and the excitation functions in different bins of the  $\eta$  production angle for the solutions with positive and negative product couplings are shown in Fig. 10.

The difference between the two solutions is seen very well. The solution with  $\tilde{a} > 0$  shows a strong peak at 1685 MeV for backward  $\eta$  mesons, while the solution with  $\tilde{a} < 0$  exhibits a diffractive structure. For forward  $\eta$ , the opposite holds true. The narrow  $J^P = 1/2^+$  resonance produces an asymmetry which is not supported in the data. For  $\tilde{a} < 0$  this asymmetry is partly interpreted in the fit by an increase in the contribution from the  $P_{13}$  partial wave. The narrow  $N(1685)$  interferes with the broad  $N(1710)$ , destructively in Fig. 10, left panel, and constructively in Fig. 10, right panel. Interference with other waves cannot be observed after integration over the full angular distribution.

The data clearly disfavor the scenario with a narrow  $J^P = 1/2^+$  resonance. The resulting interference with the  $J^P = 1/2^-$  wave produces the expected forward - backward asymmetry in the angular distributions, which is not reflected in the experimental data. In a further step we have determined upper limits for the quantity  $\tilde{a}$ . We find that the description of the differential cross section is still compatible with the data for  $-3 < \tilde{a} < +5$ .

### 4.3 Comparison of the quality of the two fits

In Table 1 we compare the quality of various fits. The best fit is achieved when no narrow  $N(1685)$  is imposed. In the table we give the  $\chi^2$  per data point for the differential cross section [19] and for the beam asymmetry [41]. The mass range for which the  $\chi^2$  is calculated is restricted to 1610 – 1710 MeV, the range which is most relevant for the existence of  $N(1685)$ . Fits are performed using the statistical errors only and the statistical and systematic error added quadratically.

The fit in which no narrow  $N(1685)$  is imposed gives the best  $\chi^2$  and is our favored fit. It is shown in Figs. 11

as solid curve. The differential cross sections are perfectly described; the beam asymmetry at 1586 MeV shows a few points which are missed by the fit but in the next energy bin, fit and data are already fully consistent. In contrast to these findings, the fit with enforced contributions from a narrow  $N(1685)$  exhibits significant deviations from data. In these fits, the  $N(1685)$  mass is constrained by  $1660 < M < 1710$  MeV, the width by  $\Gamma < 35$  MeV while the product branching ratio is fixed to  $\tilde{a} = \sqrt{Br(\eta n)}A_n^{1/2} = \pm 12 \text{ GeV}^{-\frac{1}{2}} 10^{-3}$ . Both solutions (with positive and negative  $\tilde{a}$ ) provide a strong backward-forward asymmetry in the angular distributions which is not supported by the data. To compensate this asymmetry the fit increased the contribution from the  $J^P = 3/2^+$  partial wave. However, it leads to a deterioration for the description of the GRAAL beam asymmetry data. The differential cross section in the mass region 1600 - 1720 MeV and the GRAAL beam asymmetry data are compared with different fits in Fig. 11. The fits return the masses listed in Table 1 while the width goes to the boundary value. In one of the fits (not shown),  $\tilde{a}$  was defined as a complex number with  $|\tilde{a} = 12| \text{ GeV}^{-\frac{1}{2}} 10^{-3}$ . The fit gave a marginal overall improvement.

Finally, we determine upper limits for contributions. For  $\tilde{a} = 5$ , first visible deviations between data and fit show up and the total  $\chi^2$  increases by slightly more than 25, corresponding to  $5\sigma$ . Similar discrepancies are observed for  $\tilde{a} = -3$ . We conclude that – if a narrow  $N(1685)$  exists in the  $J^P = 1/2^+$  wave – its production and decay branching fractions must obey  $-3 < \tilde{a} < 5$ .

Numerically, the fit converges to helicity amplitudes given in Table 2. Obviously, the two  $J^P = 1/2^-$  resonances interfere differently. The helicity ratios for the  $\eta$ -photoproduction off protons, recent data on the double-polarization variables  $F$  and  $T$  from MAMI [42] and on  $E, G, T, P, H$  from ELSA [43] are included.

For the proton the helicity couplings of both states have like sign, for the neutron opposite sign. However, the hadronic phase involved in the  $N^* \rightarrow N\eta$  decay of the two states (with respect to pion production) is predicted

**Table 2.** Helicity amplitudes determined from a fit without a narrow  $N(1685)$  resonance. The T-matrix couplings are those which are listed in the RPP. K-matrix couplings are reproduced as small numbers. The results of a fit to the 2002 data using the Single-Quark-Transition model [47] are shown for comparison.

		$N(1535)1/2^-$	$N(1650)1/2^-$		$N(1535)1/2^-$	$N(1650)1/2^-$			
$p$	T-matrix	$0.114 \pm 0.008$	$0.032 \pm 0.007$	$\text{GeV}^{-1/2}$	$n$	T-matrix	$-0.095 \pm 0.006$	$0.019 \pm 0.006$	$\text{GeV}^{-1/2}$
	Phase	$10 \pm 5^\circ$	$-2 \pm 11^\circ$			Phase	$8 \pm 5^\circ$	$0 \pm 15^\circ$	
	K-matrix	$0.096 \pm 0.007$	$0.075 \pm 0.007$			K-matrix	$-0.120 \pm 0.006$	$-0.052 \pm 0.006$	
	SQT	$0.097 \pm 0.007$	$0.053 \pm 0.004$			SQT	$-0.090 \pm 0.006$	$-0.031 \pm 0.003$	

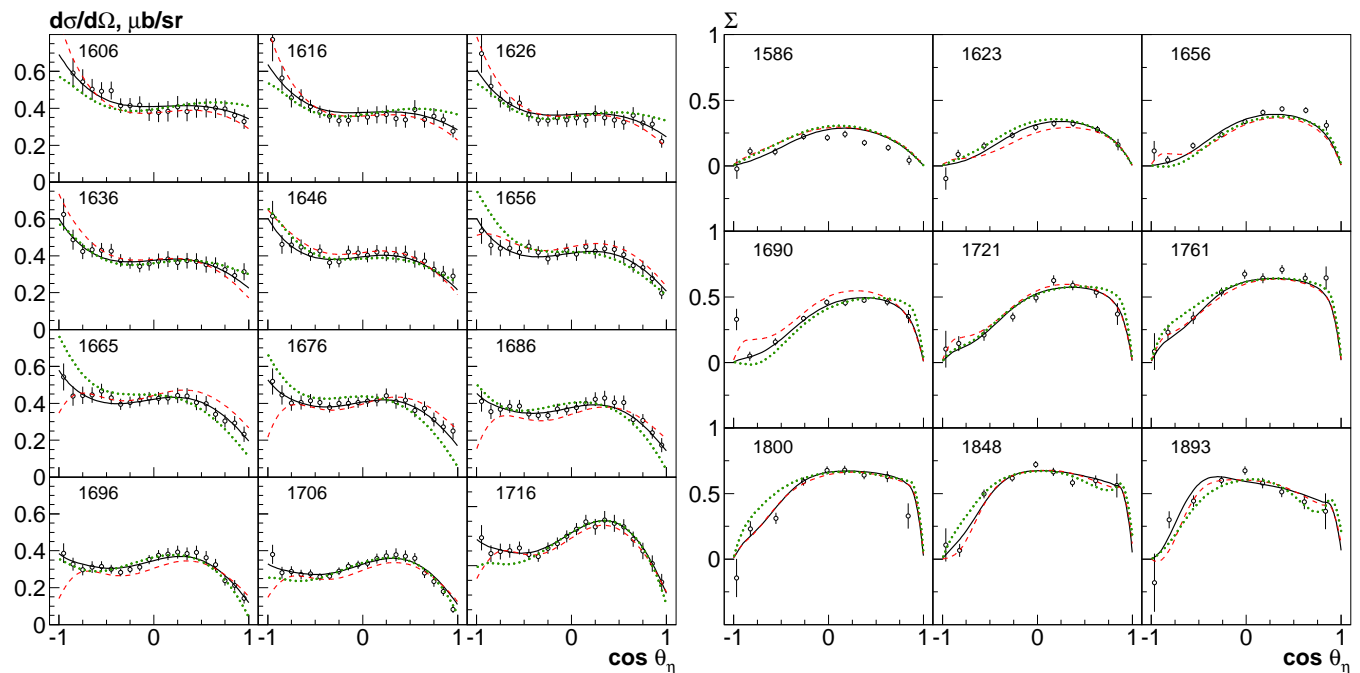


**Fig. 11.** (color online) Differential cross section (left) and beam asymmetry (right) for the eta photoproduction off neutrons. The numbers correspond to the central mass of a bin (in MeV). The solution with  $J^P = 1/2^-$  interference is shown as black curves, the solution with  $N(1680)1/2^+$  state with negative  $\eta n$  coupling as dashed (red) curves, and the solution with positive coupling as dotted (green) curves.

to be positive for the  $N(1535)1/2^-$  and negative for the  $N(1650)1/2^-$  [44]; experimentally, the  $\pi N \rightarrow N^* \rightarrow \eta N$  transition residue has a phase of  $-(76 \pm 5)^\circ$  for  $N(1535)1/2^-$  and  $+134 \pm 10^\circ$  for  $N(1650)1/2^-$  [35]; their relative phase is hence  $+(210 \pm 12)^\circ$  close to the predicted  $180^\circ$ . Hence the resulting interference is destructive for the reaction  $\gamma p \rightarrow \eta p$  and constructive for  $\gamma n \rightarrow \eta n$ . It was pointed out in [45] that the  $N(1650)1/2^-$  helicity amplitude is at variance with model predictions (see, e.g., [32] for references to predictions), and in particular that the positive sign of the  $N(1650)1/2^-$  helicity amplitude is unexpected. It was shown that the value implies that the  $N(1650)1/2^-$  must have a large  $s\bar{s}$  component.

This statement holds for the T-matrix coupling constants which give the helicity amplitudes at the pole position of the “dressed” resonance. These are complex numbers. In Table 2 we also list the K-matrix helicity amplitudes. The K-matrix pole characterizes the position of

the pole when all decay modes are switched off. Thus, the K-matrix poles can be interpreted as pole position of the “undressed” resonance. In the neighborhood of important thresholds - in this case of the  $K\Lambda$  threshold - T-matrix and K-matrix coupling constants can differ substantially. The helicity amplitudes of the “undressed”  $N(1650)1/2^-$  resonance are real numbers. The “undressed” helicity amplitudes are in good qualitative agreement with the predictions of the Single-Quark-Transition model [47] and do not necessitate a large  $s\bar{s}$  component in the  $N(1650)1/2^-$  wave function.

#### 4.4 Interference in the $J^P = 1/2^-$ wave in $\gamma n \rightarrow \pi^0 n$

We now ask if a trace of the controversially discussed  $N(1685)$  can be found in the reaction  $\gamma n \rightarrow \pi^0 n$ . In this

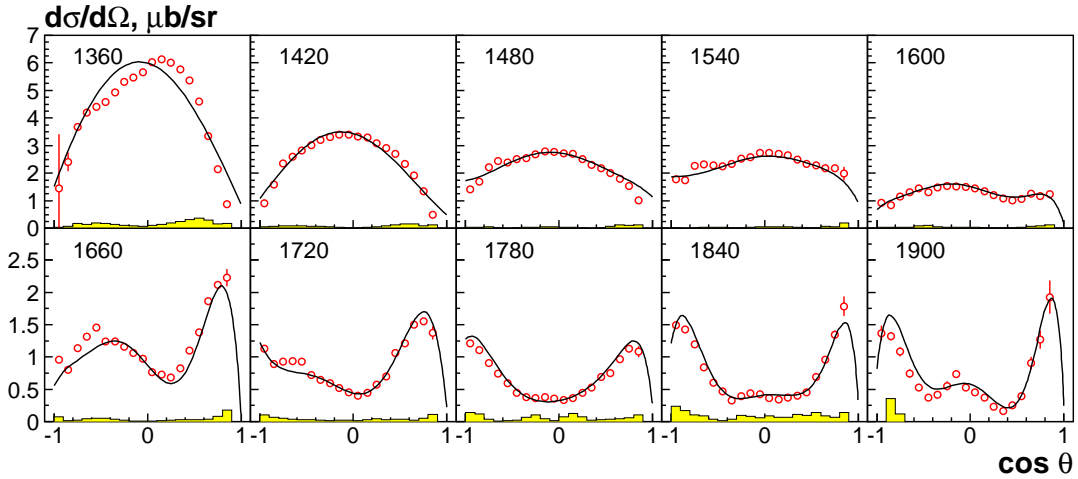


**Fig. 12.** Differential cross sections for  $\gamma n \rightarrow \pi^0 n$  [34]. The solid curve shows the BnGa fit to the data. The statistical errors are mostly smaller than circles representing the data. The systematic errors are shown as yellow histograms.

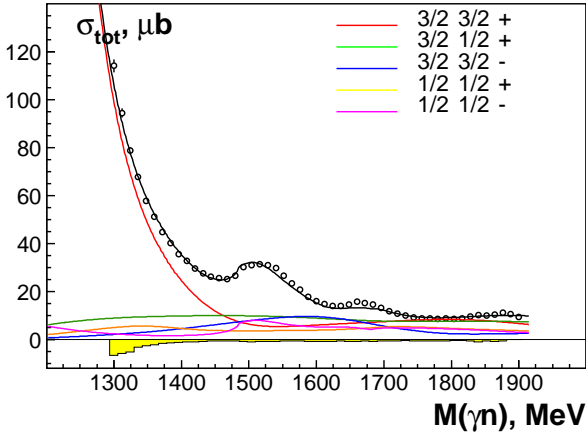


**Fig. 13.** (color online) The total cross section for  $\gamma n \rightarrow \pi^0 n$  [34]. The black curve shows the BnGa fit to these data, the colored curves the contributions from different partial waves  $J^P$  with isospin 1/2 and 3/2.

case, the final state consists of a proton, a neutron, and a pion (instead of an  $\eta$ ). The data are much stronger influenced by final state interactions than  $\eta$ -photoproduction [34]. With this warning we show in Fig. 12 the differential cross section and in Fig. 13 the total cross section for  $\gamma n \rightarrow \pi^0 n$  measured with the Crystal Ball/TAPS calorimeter at the MAMI accelerator [34]. At low energy, the reaction is dominated by  $\Delta(1232)$  production; its tail exceeds all other contributions up to an invariant mass of 1450 MeV. The peak in the second resonance region is mainly assigned to  $N(1520)3/2^-$ , the small peak below 1700 MeV to  $N(1680)5/2^+$ . The figure also displays the contribution of the  $J^P = 1/2^-$  wave to the total cross section. The contribution is small and shows the opening of the  $\eta n$  threshold. In the mass region of interest (at 1680 MeV) the contribution shows no significant feature.

#### 4.5 $N(1685)$ in Compton scattering

A trace of  $N(1685)$  may have been found in the  $\gamma n \rightarrow \gamma n$  total cross section [22] and in the beam asymmetry for  $\gamma p \rightarrow \gamma p$  [23]. We do not see how the two phenomena could possibly be related to the interference pattern in the  $\gamma n \rightarrow \eta n$  discussed in this paper.

## 5 Discussion and Summary

We have scrutinized the evidence for the existence of a narrow resonance at 1685 MeV. A structure at this mass was reported from different reactions: i) a very significant bump at this mass in the  $\gamma n \rightarrow \eta n$  total cross section was observed in three experiments, at GRAAL [2], ELSA [3, 4], and MAMI [10,19]; ii) the reaction  $\gamma p \rightarrow \eta p$  showed a small anomaly at 1685 MeV [21]; and iii) an excess of events at about this mass was observed in Compton scattering  $\gamma n \rightarrow \gamma n$  [22]. The beam asymmetry for  $\gamma p \rightarrow \gamma p$  [23] reported two structures, one at 1680 MeV. Intriguingly, the observed properties of the structure - when interpreted as a resonance - agreed very well with predictions of the soliton model for the non-strange member of a  $J^P = 1/2^+$  antidecuplet of pentaquark states.

i) The new and very precise data from MAMI enabled us to a much more solid partial-wave analysis of the  $\gamma n \rightarrow n\eta$  reaction. Our fit results show that the bump in the total cross section and also the behavior of the angular distributions can be understood quantitatively as interference between the two well-known resonances in the  $J^P = 1/2^-$  wave, the  $N(1535)1/2^-$  and the  $N(1650)1/2^-$  states. This fit requires, however, that the sign of the electromagnetic  $A_{1/2}$  helicity coupling of the  $N(1650)1/2^-$  is inverted for the neutron with respect to the current PDG [5] entry and also with respect to an early analysis in the framework of the BnGa model [27] (but in agreement with a later BnGa analysis [32]). When a narrow  $N(1685)1/2^+$  resonance was enforced in the model, the quality of the fit deteriorated

significantly. Consequently, there is no evidence for such a state from  $\gamma n \rightarrow n\eta$ . It is worthwhile to mention that none of the papers reporting evidence for the structure took the interference between the two  $J^P = 1/2^-$  resonances into account when fitting the data. The  $p$  and  $n$  helicity couplings of  $N(1650)1/2^-$  determined here imply, however, that the  $N(1650)1/2^-$  resonance should have a large  $s\bar{s}$  component in its wave function [45]. This conclusion is avoided when the K-matrix poles are interpreted as “undressed” resonance and the K-matrix couplings are confronted with models. The “dressed” helicity amplitudes are not in conflict with model calculations.

ii) The angular distributions show that the bump in the total cross section is an S-wave phenomenon; it is not a P-wave enhancement.

iii) The anomaly at 1685 MeV in the total cross section of the reaction  $\gamma p \rightarrow \eta p$  reported in [21] could be traced quantitatively to the opening of the  $K \Sigma$  threshold. Since data on  $\gamma p \rightarrow K \Sigma$  are included in the Bonn-Gatchina partial wave analysis, there is no free parameter available to fit the shape of the anomaly in the  $\gamma p \rightarrow \eta p$  cross section. The small size of this anomaly rules out the possibility that the  $K \Sigma$  threshold might be responsible for the narrow bump observed in the  $\gamma n \rightarrow \eta n$  total cross section.

iv) The small excess in the number of events in Compton scattering  $\gamma n \rightarrow \gamma n$  [22] at 1680 MeV. A study of the beam asymmetry  $\Sigma$  for Compton scattering off protons reported two narrow structures with masses near 1680 and 1.720 MeV [23]. Their origin needs further clarification.

We would like to thank M. Dieterle for providing the data on  $\gamma n \rightarrow \pi^0 n$  in numerical form. We acknowledge support from the Deutsche Forschungsgemeinschaft (within the SFB/TR16), the Schweizerische Nationalfonds, and the Russian Foundation for Basic Research.

## References

1. B. Krusche, *Eur. Phys. J. Special Topics* **198**, 199 (2011).
2. V. Kuznetsov *et al.*, *Phys. Lett. B* **647**, 23 (2007).
3. I. Jaegle *et al.* [CBELSA/TAPS Collaboration], *Phys. Rev. Lett.* **100**, 252002 (2008).
4. I. Jaegle *et al.*, *Eur. Phys. J. A* **47**, 89 (2011).
5. K. A. Olive *et al.* [Particle Data Group Collaboration], *Chin. Phys. C* **38**, 090001 (2014).
6. D. Diakonov, V. Petrov, and M. V. Polyakov, *Z. Phys. A* **359**, 305 (1997).
7. M. V. Polyakov and A. Rathke, *Eur. Phys. J. A* **18**, 691 (2003).
8. V. Kuznetsov and M. V. Polyakov, *JETP Lett.* **88**, 347 (2008).
9. R.A. Arndt *et al.*, *Phys. Rev. C* **69**, 035208 (2004).
10. D. Werthmüller *et al.*, *Phys. Rev. C* **90**, 015205 (2014).
11. Y.I. Azimov *et al.*, *Eur. Phys. J. A* **25** 325 (2005).
12. See V. D. Burkert, *Int. J. Mod. Phys. A* **21**, 1764 (2006).
13. K. H. Hicks, *Eur. Phys. J. H* **37**, 1 (2012).
14. T. Liu, Y. Mao and B. Q. Ma, *Int. J. Mod. Phys. A* **29**, no. 13, 1430020 (2014).
15. T. Nakano *et al.* [LEPS Collaboration], *Phys. Rev. C* **79**, 025210 (2009).
16. M. J. Amarian, G. Gavalian, C. Nepali, M. V. Polyakov, Y. Azimov, W. J. Briscoe, G. E. Dodge and C. E. Hyde *et al.*, *Phys. Rev. C* **85**, 035209 (2012).
17. M. Anghinolfi, J. Ball, N. A. Baltzell, M. Battaglieri, I. Bedlinskiy, M. Bellis, A. S. Biselli and C. Bookwalter *et al.*, *Phys. Rev. C* **86**, 069801 (2012).
18. V. V. Barmin *et al.* [DIANA Collaboration], *Phys. Rev. C* **89**, 045204 (2014).
19. D. Werthmüller *et al.* [A2 Collaboration], *Phys. Rev. Lett.* **111**, 232001 (2013).
20. L. Witthauer *et al.*; *Eur. Phys. J. A* **47**, 89 (2013).
21. E. F. McNicoll *et al.* [Crystal Ball at MAMI Collaboration], *Phys. Rev. C* **82**, 035208 (2010) [Erratum-ibid. *C* **84**, 029901 (2011)].
22. V. Kuznetsov *et al.*, *Phys. Rev. C* **83**, 022201 (2011).
23. V. Kuznetsov *et al.*, *Phys. Rev. C* **91**, no. 4, 042201 (2015).
24. Ki-Seok Choi *et al.*, *Phys. Lett. B* **636** 253 (2006) 253.
25. A. Fix, L. Tiator, and M.V. Polyakov, *Eur. Phys. J. A* **32** 311 (2007).
26. M. Shrestha and D.M. Manley, *Phys. Rev. C* **86** 045204 (2012), *idem* **86** 055203 (2012).
27. A. V. Anisovich *et al.*, *Eur. Phys. J. A* **41**, 13 (2009).
28. V. Shklyar, H. Lenske, and U. Mosel, *Phys. Lett. B* **650** 172 (2007).
29. R. Shyam and O. Scholten, *Phys. Rev. C* **78** 065201 (2008).
30. M. Döring and K. Nakayama, *Phys. Lett. B* **683** 145 (2010).
31. X. -H. Zhong and Q. Zhao, *Phys. Rev. C* **84**, 045207 (2011).
32. A. V. Anisovich *et al.*, *Eur. Phys. J. A* **49**, 67 (2013).
33. A. V. Anisovich, E. Klempt, V. A. Nikonov, A. V. Sarantsev and U. Thoma, “Comment on ”Narrow Structure in the Excitation Function of  $\eta$  Photoproduction off the Neutron”,” arXiv:1402.7164 [nucl-ex].
34. M. Dieterle *et al.*, *Phys. Rev. Lett.* **112**, 142001 (2014).
35. A. V. Anisovich *et al.*, *Eur. Phys. J. A* **48**, 15 (2012).
36. A. V. Anisovich *et al.*, *Eur. Phys. J. A* **49**, 158 (2013).
37. A. V. Anisovich *et al.*, *Phys. Lett. B* **719**, 89 (2013).
38. V. Kuznetsov, M. V. Polyakov, and M. Thurmman, *JETP Lett.* **94**, 503 (2011).
39. D. Rönchen *et al.*, *Eur. Phys. J. A* **49**, 44 (2013).
40. M. Döring, *AIP Conf. Proc.* **1432**, 297 (2012).
41. A. Fantini *et al.*, *Phys. Rev. C* **78**, 015203 (2008).
42. C. S. Akondi *et al.* [A2 at MAMI Collaboration], *Phys. Rev. Lett.* **113**, 102001 (2014).
43. J. Müller *et al.* [CBELSA/TAPS Collaboration], in preparation.
44. S. Capstick and W. Roberts, *Phys. Rev. D* **49** (1994) 4570.
45. T. Boika, V. Kuznetsov and M. V. Polyakov, arXiv:1411.4375 [nucl-th].
46. Y. Wada, K. Egawa, A. Imanishi, T. Ishii, S. Kato, K. Ukai, F. Naito and H. Nara *et al.*, *Nucl. Phys. B* **247**, 313 (1984).
47. V. D. Burkert, R. De Vita, M. Battaglieri, M. Ripani and V. Mokeev, *Phys. Rev. C* **67**, 035204 (2003)